Available online at www.sciencedirect.com

ScienceDirect

Journal of Ocean Engineering and Science 1 (2016) 84–91

www.elsevier.com/locate/joes

Nonlinear roll damping of a barge with and without liquid cargo in spherical tanks

Wenhua Zhao[a,*], Mike Efthymiou[a], Finlay McPhail[b], Sjoerd Wille[b]

[a] *Faculty of Engineering, Computing and Mathematics, The University of Western Australia, 35 Stirling Highway, Crawley, WA 6009, Australia*
[b] *Shell Global Solutions BV (Shell), Kessler Park 1, 2280 AB, Rijswijk, The Netherlands*

Received 1 June 2015; received in revised form 3 July 2015; accepted 19 July 2015
Available online 29 January 2016

Abstract

Damping plays a significant role on the maximum amplitude of a vessel's roll motion, in particular near the resonant frequency. It is a common practice to predict roll damping using a linear radiation–diffraction code and add that to a linearized viscous damping component, which can be obtained through empirical, semi-empirical equations or free decay tests in calm water. However, it is evident that the viscous roll damping is nonlinear with roll velocity and amplitude. Nonlinear liquid cargo motions inside cargo tanks also contribute to roll damping, which when ignored impedes the accurate prediction of maximum roll motions. In this study, a series of free decay model tests is conducted on a barge-like vessel with two spherical tanks, which allows a better understanding of the nonlinear roll damping components considering the effects of the liquid cargo motion. To examine the effects of the cargo motion on the damping levels, a nonlinear model is adopted to calculate the damping coefficients. The liquid cargo motion is observed to affect both the linear and the quadratic components of the roll damping. The flow memory effect on the roll damping is also studied. The nonlinear damping coefficients of the vessel with liquid cargo motions in spherical tanks are obtained, which are expected to contribute in configurations involving spherical tanks.

Keywords: LNG carrier; Nonlinear roll damping; Liquid cargo motion; Spherical tanks; Model test.

1. Introduction

Floating Liquefied Natural Gas (FLNG) [21] is a new floating-structure concept which combines upstream facilities for liquefying natural gas at -162 ºC, storage of the liquefied gas in cargo tanks and offloading it into LNG Carriers. Side-by-side offloading has been identified as a promising configuration between LNG Carriers and the FLNG vessel for offtake of LNG. In this concept, LNG carriers that would normally be berthed against a jetty on the coast, or in ports with break waters, are now required to lift cargo in the open seas. Due to the close proximity between FLNG and the LNG carrier and the weathervaning capability of the FLNG, the operation is sensitive to the roll motions of the two vessels. The carrier roll motions may, as a consequence, dominate the availability in some regions. A reliable prediction of the roll response of LNG carriers is therefore important.

Extensive studies on this problem have been conducted during the past decades. For roll motions of a small amplitude, a linear formulation can provide more or less reliable predictions (Blagoveshchenskiĭ [1]; Salvesen et al. [13]). However, as the response amplitude becomes large, nonlinearities become significant, necessitating a nonlinear formulation [2]. One possible nonlinear contribution could be accounted for by introducing nonlinear restoring coefficients [5] that are dependent on the shape of the stability diagram [16]. However, it is unable to match completely with experimental data by solely considering nonlinear restoring moments (Denise [5]; Robinson and Stoddart [12]). To achieve a complete match, viscous damping needs to be included. In contrast, nonlinear restoring force seems not necessary when the nonlinear damping effects have been accounted for. As a consequence, it is therefore essential to better understand the damping levels for a reliable prediction of the roll motions of a vessel.

* Corresponding author. Tel.: +61 08 64883122.
E-mail address: wenhua.zhao@uwa.edu.au (W. Zhao).

http://dx.doi.org/10.1016/j.joes.2015.12.002

To predict the viscous damping of roll motions, Tanaka [15] developed a semi-empirical method. Following that, Ikeda et al. [8] conducted a comprehensive series of experimental studies. In their study, they divided the roll damping into several components and developed a method for predicting the roll damping. Each component is predicted theoretically if possible, otherwise empirically. 26 years later, Ikeda [9] improved his empirical formula to be able to determine the damping coefficients for ships considering forward speed. In addition, Chakrabarti [4] examined the roll damping components and explained the empirical formulas for various types of roll damping, which are helpful for prediction of roll damping. For engineering purposes, the roll motion of a floating structure can be predicted more or less reliably using semi-empirical and empirical methods [6]. It should be noted that this does not mean the roll motion problem has been solved. In contrast, more research is necessary in this area [7].

To the authors' knowledge, all existing studies focus on the viscous damping associated with the outer hull of a floating structure or ship without free-surface effects. In other words, the possible effect of liquid cargo motions inside tanks has not been considered. However, the liquid cargo motions may play a significant role in the roll damping, which further affects the operational window for side-by-side offloading of FLNG facilities. It is of significant value, therefore, to examine the roll damping contributions from the liquid cargo motions and to understand better the roll damping level by incorporating a contribution from the liquid cargo motions inside tanks.

In this study, a series of experiments are carried out with a vessel model fitted with spherical tanks. Several roll-decay tests have been performed. The tanks are filled with water to represent partially-filled conditions. To identify the effects of the liquid cargo motion on the roll damping level, additional sets of runs were performed for which the tanks were empty, but the vessel properties modified to result in a 'frozen' approximation of the partially-filled condition. To provide a basis for numerical simulations, we demonstrate the roll damping levels of the vessel in various partially-filled conditions. The memory effect of liquid flow is studied through free decay tests with different initial exciting amplitudes.

2. Theoretical background

Assuming that there is no coupling from motions at other degrees of freedom, a typical roll motion equation considering nonlinear roll damping can be written as follows [3,14,16,18]:

$$(M+A)\ddot{\varphi} + B_L\dot{\varphi} + B_N\dot{\varphi}|\dot{\varphi}| + K\varphi = M(t), \tag{1}$$

where φ, $\dot{\varphi}$, and $\ddot{\varphi}$ are the roll angle, angular velocity, and angular acceleration. $M$and A refer to the displacement and added mass moments of inertia in roll. K is the restoring coefficient and $M(t)$ is the exciting moment by external force, which equals zero in a free decay test in calm water. B_L and B_N represent the linear and quadratic damping coefficients, respectively.

2.1. Linear damping model

The non-dimensional equation of the roll motion for the free decay tests considering solely linear damping can be written as:

$$\ddot{\varphi} + 2\xi\omega_n\dot{\varphi} + \omega_n^2\varphi = 0, \tag{2}$$

where ξ is the ratio of linear damping B_L to critical damping $B_{crit} = 2\cdot\sqrt{(M+A)\cdot K}$, and ω_n is the natural frequency of the roll motion, which can be expressed as $\omega_n = \sqrt{K/(M+A)}$.

A general solution for Eq. (2) can be written in the following form:

$$\varphi(t) = e^{-\xi\omega_n t}(k_1\cos\omega_d t + k_2\sin\omega_d t), \tag{3}$$

where k_1 and k_2 are constants, which can be determined by initial conditions. ω_d is the damped natural frequency of the oscillations in water (including the damping effects). ω_d can be expressed through:

$$\omega_d = \omega_n\sqrt{1-\xi^2}. \tag{4}$$

Defining the interval between two successive peaks (or troughs) as the natural period, T_n, of the oscillations and substituting Eq. (4) into Eq. (3), one can obtain the relationship between the values of two subsequent peaks in the decaying motion signal through the following equation:

$$\frac{\varphi_i}{\varphi_{i+1}} = e^{\xi\omega_n\frac{T_n}{2}} = e^{\xi\pi}, \tag{5}$$

where φ_i and φ_{i+1} are the motion amplitudes of the i^{th} and $(i+1)^{th}$oscillations. The non-dimensional damping coefficient can therefore be expressed as the following equation:

$$\xi = \frac{1}{\pi}\frac{\ln\varphi_i - \ln\varphi_{i+N}}{N}, \tag{6}$$

where N is the number of oscillations. Based on Eq. (6), the variations of damping coefficients with respect to the roll response amplitudes can be easily plotted. To distinguish with the following one, the damping coefficient obtained by this approach is referred to as classical damping [19].

2.2. Nonlinear damping model

To evaluate the nonlinear damping term B_N in the roll motion Eq. (1), it is assumed [3,10] that the decaying oscillation is reasonably harmonic over each half cycle. Therefore, the nonlinear term is linearized by a Fourier series expansion as:

$$\dot{\varphi}|\dot{\varphi}| = \frac{8}{3\pi}\omega_n\varphi_i\dot{\varphi}, \tag{7}$$

As a consequence, the non-dimensional nonlinear equitation of roll motion can be written as:

$$\ddot{\varphi} + 2\zeta\omega_n\dot{\varphi} + \eta\frac{8}{3\pi}\omega_n\varphi_i\dot{\varphi} + \omega_n^2\varphi = 0, \tag{8}$$

where η is the non-dimensional form of the nonlinear term B_N $(\eta = B_N/(M+A))$.

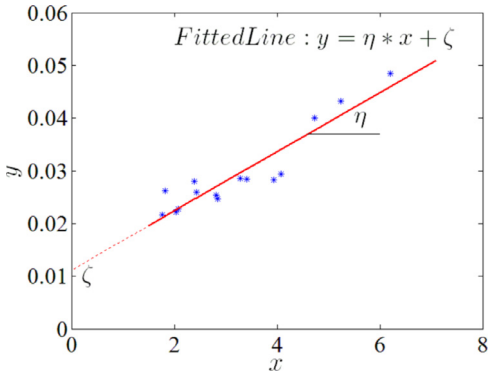

Fig. 1. Illustration of the nonlinear roll damping model: the blue stars refer to the left side of Eq. (9) ($\frac{1}{\pi}\frac{\ln\varphi_{i-1}-\ln\varphi_{i+1}}{2}$), the solid red line refers to the fitted line of the blue stars.

Table 1
Vessel configuration.

Designation	Full scale	Model scale
Length between perpendiculars (m)	200	3.333
Breadth (m)	46	0.767
Depth (m)	25.5	0.425

By a similar analogy with the linear case in Eq. (6), we easily obtain the following equation for the nonlinear case:

$$\frac{1}{\pi}\frac{\ln\varphi_{i-1}-\ln\varphi_{i+1}}{2}=\zeta+\frac{4}{3\pi}\eta\varphi_i, \tag{9}$$

Which is the equation of a straight line with the left-hand side representing the vertical axis and φ_i referring to the horizontal axis. The measured peak values of the oscillations can be fitted to a straight line by the least square method, in which the intercept and slope are ζ and η, respectively. In such a case, $\zeta$and η represent the coefficients of the linear and quadratic components, respectively, as illustrated in Fig. 1.

3. Model particulars

The barge-like vessel model was designed to possess similar roll characteristics to those of a typical Moss-type LNG carrier. The model tests are conducted at the Deepwater Offshore Basin in Shanghai Jiao Tong University at the model scale of 1:60. Two spherical tanks were mounted on board the vessel. The main geometric characteristics of the vessel are listed in Table 1 at both full scale and model scale. The corresponding lines drawing of the vessel is plotted in Fig. 2 and the fabricated model is shown in Fig. 3.

In this study, free decay tests of the vessel in five different volumetric loaded conditions were considered, namely 0% (ballast), 25%, 50%, 75% and 100% (fully loaded). In the 0% loaded condition, there is no liquid in the spherical tanks. In the 100% loaded condition, the spherical tanks are full of liquid, thus there is no free surface inside the tanks. With regard to the intermediate loaded conditions such as 25%, 50% and 75%, there are free surfaces inside the spherical tanks. The inertia parameters of the vessel are shown in Table 2.

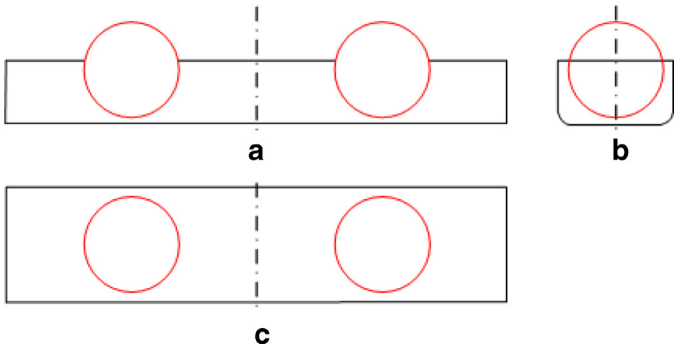

Fig. 2. Lines drawing of the vessel with two spherical tanks: (a) front view, (b) side view, (c) top view.

Fig. 3. Scale model used in experiments.

4. Experimental set-ups

Prior to the model tests, the vessel model was adjusted to achieve the inertia parameters without liquid cargo shown in Table 2. After that, the spherical tanks were filled with fresh water up to the required filling levels so that model tests could be conducted. It should be noted that there was a frozen cargo case for the vessel model under the 50% loaded condition. In this case, steel weights were used to achieve the target inertia parameters. This was achieved by matching the natural period with that in the liquid cargo case.

In the decay tests, a heeling moment was applied manually to the model so that the model could reach the target heel angle slowly. During this procedure, the displacement of the model was monitored through the motion measurement system. This monitoring data enabled us to ensure that the model moved freely with a minimum of initial pitch and heave excitations. When the initial heeling angle (as shown in Fig. 4) reached the target value, the vessel was quickly released and moved freely in the calm water. The resulting roll motions were recorded simultaneously. The recorded time traces were used for the analyses of the nonlinear roll damping.

Table 2
Inertia parameters of the vessel in five different filling conditions at full scale.

Designation	Filling levels				
	0%	25%	50%	75%	100%
Mena draft (m)	9.17	10.19	11.10	11.20	11.20
Displacement weight (t)	81482.83	90859.18	99297.90	100235.53	100235.53
Prior to cargo loading					
Radius of roll gyration (m)	19.80	19.60	19.40	18.80	15.80

Note: The vessel is assumed to be floating in fresh water and the spherical tanks are assumed to be filled with fresh water.

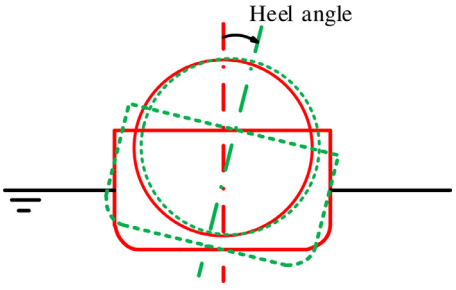

Fig. 4. Schematic of the decay tests in calm water.

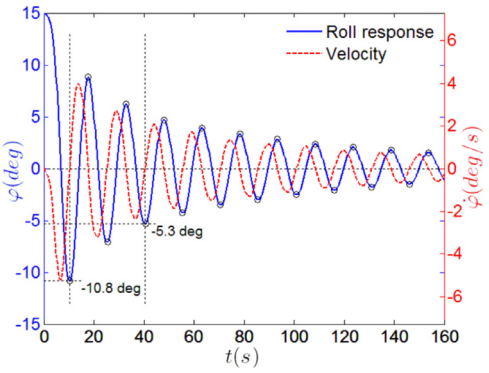

Fig. 5. Roll decay curve in calm water and its corresponding velocity: the roll response crests and troughs are marked via circles.

5. Results and discussion

This section discusses the damping variations against roll amplitudes, showing obvious nonlinearity. In addition, the effects of the liquid cargo motion on the roll damping levels are identified through comparison between the decay tests with and without liquid cargo motions inside tanks. To provide a basis for numerical simulations, the nonlinear roll damping coefficients of the vessel's roll motion are identified under different loaded conditions. Finally, the water surface flow memory effects and the bilge keel effects are also studied.

5.1. Nonlinearity of the roll damping

To investigate the nonlinear characteristics of roll damping, a roll decay test of the reference carrier in calm water was conducted with an initial heel angle of 15°, covering both large and small roll amplitudes. To address the nonlinearity of the roll damping and to simplify the analysis, the liquid cargo inside the spherical tanks was treated as frozen cargo using steel weights. To provide a basis for further numerical simulations, the study investigates the nonlinear roll damping performance through the damping coefficients instead of the damping moments.

The free rolling decay curve and its corresponding velocity are plotted in Fig. 5, with response peaks marked in circles. As shown in Fig. 5, the roll velocity curve shows very similar trend with the roll decay curve, with only a phase shift of 90° ahead. The amplitude-dependent linear damping coefficients have been calculated based on the theory in Section 2.1.

Fig. 6 shows the variation of damping coefficients with roll response amplitude. The damping level remains almost constant at 0.025 for the roll response amplitudes less than 4.0°.

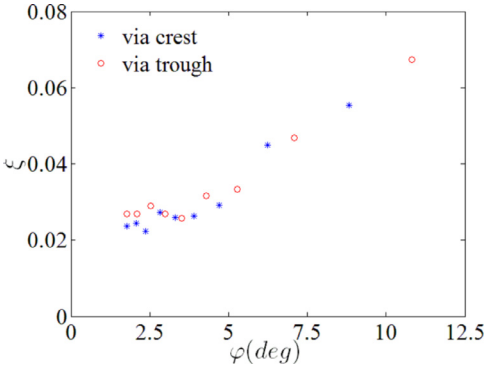

Fig. 6. Variations of the classical damping coefficients against roll oscillation amplitudes: ξ is the amplitude-dependent linear damping coefficient in Eq. (2); the blue stars refer to results from successive crests and the red dots represent those from successive troughs.

At roll amplitudes above 4.0°, the roll damping coefficient increases approximately linearly.

The damping coefficients exhibit a strong dependency on roll amplitude. For instance, the roll damping coefficient at 10.8° of roll is 0.06 which is twice the damping coefficient (0.03) at 5.3°. This indicates that the linear damping coefficient obtained according to a lower roll amplitude may be too conservative for the estimation of extreme roll motions.

Accuracy of the roll predictions may be improved by accounting for the nonlinear behavior of the roll damping. As addressed by Malta et al. [10], the quadratic damping model can generate time traces of roll decay motions that achieve better agreement with experiments than those by a linear

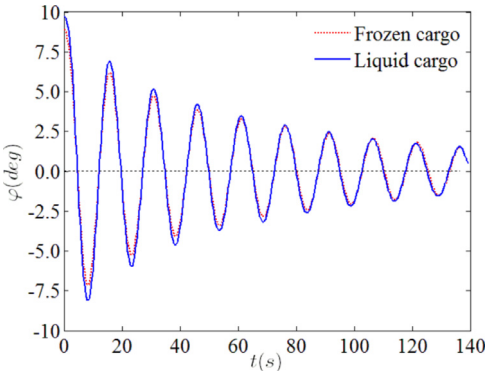

Fig. 7. Time traces of roll decay motions in the frozen and liquid cargo cases.

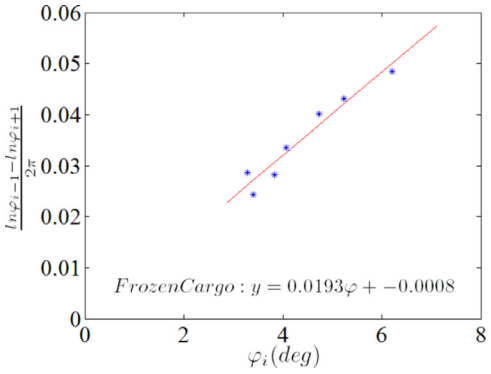

Fig. 8. Least square fit for the roll decay data with 'frozen' cargo: the intercept refers to the linear component ζ and the slope refers to the quadratic damping component η, the star points are obtained through the crests and troughs and the straight line is the fitted line.

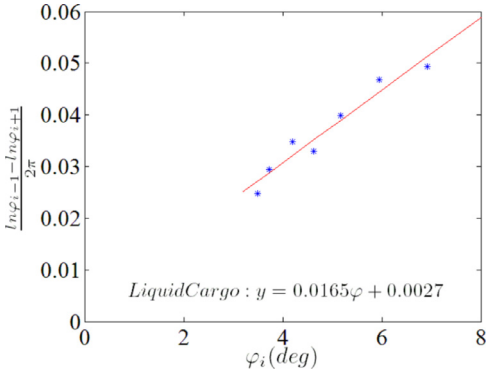

Fig. 9. Least square fit for the roll decay data with liquid cargo: the intercept refers to the linear component ζ and the slope refers to the quadratic damping component (η), the star points are obtained through the crests and troughs and the straight line is the fitted line.

damping model, in particular in the peak responses. Therefore, it will be of significant importance in practice to account for the nonlinear behavior of the roll damping, such as the estimation of operational availability. Moreover, the internal liquid cargo inside the tanks may play an important role and enhance the nonlinearity of the roll damping. A study is therefore needed of the effect of the liquid cargo motion on the roll damping levels.

5.2. Effects of the liquid cargo motion on roll damping

To clarify the effects of the liquid cargo motion on the roll damping performance, a set of tests were conducted using the barge model with liquid and frozen cargo, respectively. In the liquid cargo case, the spherical tanks are 50% filled with water, which is replaced with identical mass of steel weights for the frozen cargo case. The unique difference between the liquid and frozen cargo cases lies in the liquid flow. All the other parameters such as total mass, center of gravity and inertia parameters hold the same in static condition. The target initial heel angle for roll decay tests is set at 10° for both the liquid and frozen cargo cases.

The time traces of the roll decay tests have been plotted in Fig. 7. Here, the initial heel angle for the frozen cargo case is slightly lower than the target value (10°). This does not affect the present findings, and the reason will be addressed in detail in the following section. Fig. 7 shows that the roll amplitudes in the liquid cargo case are initially larger than those in the frozen cargo case; as time increases, the roll motions tend to have the same amplitude for the liquid and frozen cargo cases. This indicates that the liquid cargo motion affects the roll damping at larger roll amplitudes, but it has less effect at smaller roll amplitudes. This can be explained through the fact that the liquid cargo motions inside tanks produce a viscous force that damps the global roll motions. For smaller roll amplitudes, it is hard to induce significant viscous forces.

To gain a better understanding of the effects of the liquid cargo motions, the quadratic damping model illustrated in Section 2.2 is adopted to calculate the damping coefficients of the roll decay motions. Given that the liquid cargo has few effects on the roll damping at smaller roll amplitudes, the roll time traces are selected for larger roll amplitudes, say from approximately 3.5–10°. The results of the frozen and liquid cargo cases are plotted in Fig. 8 and Fig. 9, respectively. It can be seen in Fig. 8 and Fig. 9 that the quadratic roll damping coefficient decreases from 0.0193 in the frozen case to 0.0165 in the liquid case. In contrast, the linear damping component increases from approximately 0 in the frozen case to 0.0027 in the liquid case. This indicates that the liquid cargo motion inside tanks could reduce the quadratic component of the damping levels, but would amplify the linear component. It should be noted that the liquid cargo motion inside spherical tanks amplifies the classical damping levels in general, which can be observed in Fig. 7.

As per the study by Downie et al. [6], the extreme roll response is very sensitive to the damping levels in numerical simulations. Given that the extreme roll response amplitude operator near natural frequency is typical around 10° /m for a ship-like vessel, which is far from the linear value (less than 4.0°), it is advised that the nonlinear damping model be adopted in numerical predictions of extreme roll responses.

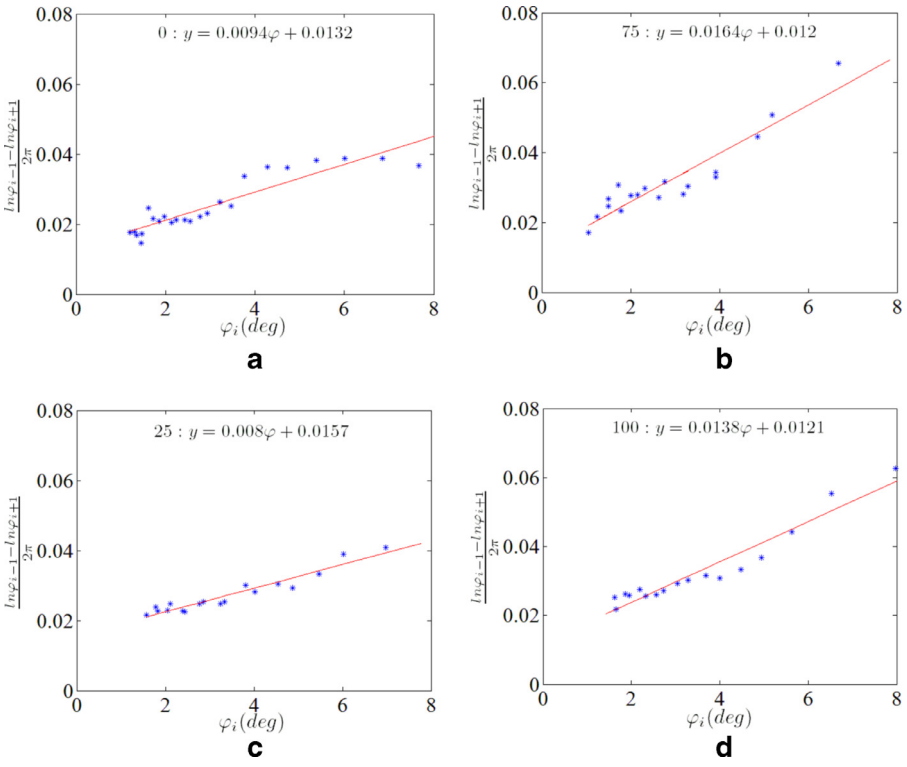

Fig. 10. Least square fits for roll decay data in different load conditions: (a) 0% load condition, (b) 25% load condition, (c) 75% load condition, (d) 100% load condition.

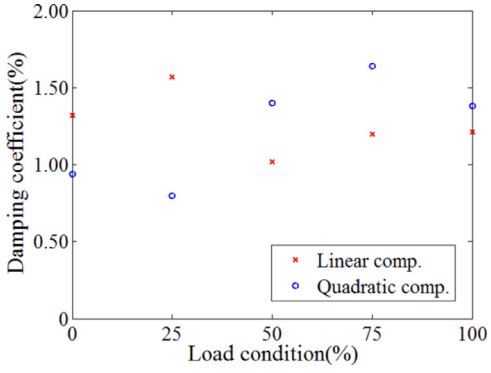

Fig. 11. Variations of the damping coefficients against load condition.

5.3. Nonlinear roll damping coefficients in different load conditions

To provide improved guidance for the analysis of LNG carrier motions, it is of importance to investigate the variations of the damping coefficients for different load conditions. In this section, the least square fits of the roll decay test data are plotted in Fig. 10 for the load conditions of 0%, 25%, 75%, and 100%. The variations of the corresponding damping coefficients (linear plus quadratic components) are plotted in Fig. 11. Among these load conditions, there is no liquid in the 0% load condition and thus no free surface, the 100% load condition represents a completely fluid-filled tank and has no free surface. The tanks in the 25% and 75% load conditions are filled with 25% and 75% of volume water.

The plots of the roll decay data in Fig. 1 once again confirm that roll damping at lower roll amplitude shows more linear behavior, with the damping becomes nonlinear as the roll amplitude increases. Consistent with a common conclusion, the critical roll amplitude for the change from linear to nonlinear roll damping is around 4.0°. Fig. 11 shows the variations of the linear and quadratic components of the roll damping against load condition. It can be seen in this figure that the load conditions have a certain effect on the weights of the linear and quadratic roll damping levels. In details, Fig. 11 shows that the linear component is larger than the quadratic component at lower load conditions, while the quadratic component gets larger than the linear component as the load conditions increase. It is worth studying whether this is general trend or specific for the tested model in this study.

5.4. Flow memory effects

It is known that [11] a memory effect is associated with the motion of a vessel which is forced to oscillate whereby the force at a given moment will depend on the previous time-history of the vessel motion. In this case, the memory effect may work through the forces induced by turbulence associated with bilge keels and the free-surface waves generated by the vessel motion. To identify if the memory effect has an influence on the freely rolling decay motions, a series of roll decay tests has been carried out for different initial heel

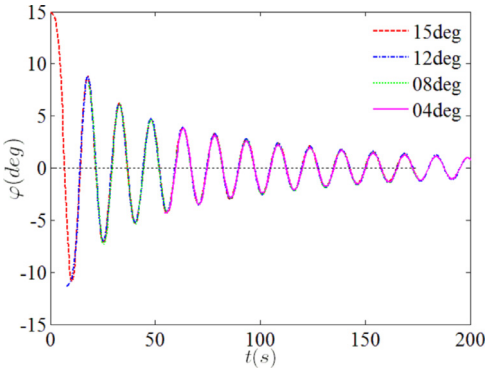

Fig. 12. Roll decay curves for different initial roll heel angles.

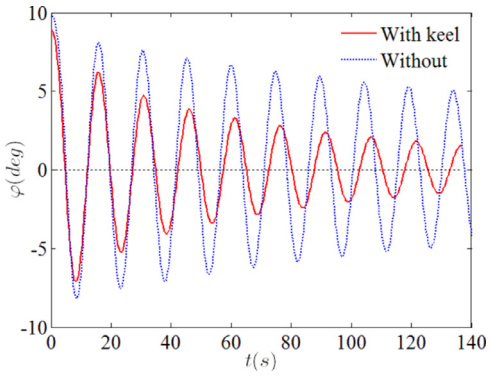

Fig. 14. Comparison of roll decay plots with and without bilge keels.

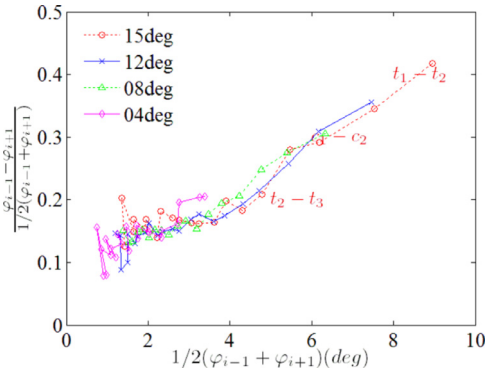

Fig. 13. Roll decay decrement plots at different initial heel angles: t_1, t_2, and t_3 represent the first three troughs, c_1 and c_2 represent the first two crests.

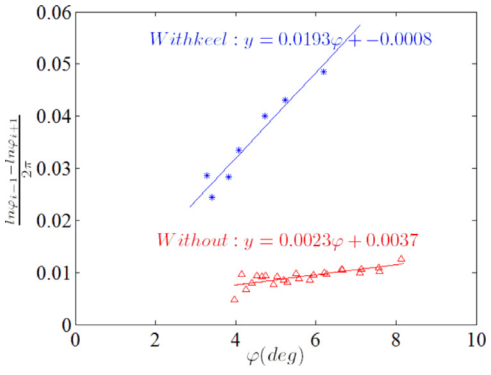

Fig. 15. Least square fits for the roll decay data of the vessel with and without bilge keels.

angles. In this section, four different initial heel angles are selected for reference, namely 15°, 12°, 8° and 4°.

The time traces of the roll decay tests are plotted in Fig. 12 for different initial heel angles. Taking the roll decay test with the initial heel angle of 4° as a reference, the model is slowly brought to the target heel angle of 4° and then released to move freely in calm water and thus there are no pre-oscillations before the decay starts. For the other cases, one can notice that there have been a number of oscillations before the roll angle reaches 4°, for example, 3.5, 3.0 and 2.5 oscillations for 15°, 12° and 8° cases, respectively. This means if we confine our attention to the time traces that are lower than 4° for the four decay curves, they represent the model oscillating with different previous time-histories of vessel motions and hence different memory conditions of the flow around the model. However, it is interesting to see that the time traces of the roll decay tests match quite well for all the cases. This indicates that the water surface flow has a negligible memory effect on the roll damping levels.

To provide a clearer way to address the water surface flow memory effects, the damping decrement results for all the different initial heel angle cases are plotted in Fig. 13. It can be seen that the damping decrements obtained for the four different initial heel angles are approximately the same with each other, both at the very beginning and the following phase of the roll decay motion. The decrement between the first two crests (ref $c_1 - c_2$) at the 15° case is approximately the same with that between the first two troughs (ref $t_1 - t_2$) at the 12° case, and the same phenomenon holds for the comparison between the 12° case, the 8° case and the 4° case. This indicates that the pre-oscillations do not have a visible effect on the following time traces in roll decay.

5.5. Bilge keel effects

It has been a common practice to use bilge keels to reduce roll responses of a vessel [20]. In this section, the bilge keel effect is quantitatively studied. In particular, the effects of the bilge keels on the linear and quadratic components of roll damping are studied. To achieve this, the roll decay tests of the vessel in the 50% load condition with frozen cargo inside the tanks were conducted with and without bilge keels, respectively.

In Fig. 14, the time traces of the roll decay motions are shown for the vessel with and without bilge keels. It can be seen in Fig. 14 that the roll period of the vessel has been changed when removing the bilge keels. This is related to the fact that the damping levels in the two cases are significantly different. As addressed in Eq. (4), the damped roll frequency is dependent on the damping level in roll motions. The different damping levels therefore result in different damped roll oscillation frequencies. To understand better the effects of the bilge keels on the nonlinear roll damping, the least square fits for the roll decay data are plotted in Fig. 15.

As shown in Fig. 15, the damping data for the vessel with bilge keels are much larger than those for the vessel without bilge keels, which indicates that the bilge keels play a significant role in roll damping. In the bilge keel case, the quadratic damping component dominates the roll damping, whereas there are identical values for the linear and quadratic damping components for the roll decay data without bilge keels. The least square fit for the roll decay data without bilge keels is almost a horizontal curve. This means that the roll damping is almost linear without bilge keels. Through a comparison of the parameters of the two fitted lines, one can find that the quadratic component of roll damping decreases significantly from 0.0193 with bilge keels to 0.0023 without bilge keels, while the linear component increases slightly from 0 to 0.0037. This means that the bilge keels mainly affect the roll damping through the quadratic component and its effect on the linear component is less important.

Another interesting phenomenon can be seen in Fig. 15 is that the fitted data with bilge keels show better convergence than those without bilge keels. A possible reason for this phenomenon could be associated with the effects of the disturbances [17] that occur near the vessel if there are bilge keels, but disappear when the bilge keels are removed.

6. Conclusions

Taking account of the liquid cargo motions inside the spherical tanks, a series of experiments has been conducted which focuses on the nonlinear roll damping characteristics of an LNG carrier. The effects of the liquid cargo motions on the nonlinear roll damping levels have been clarified. The main conclusions are listed as follows:

- The roll damping coefficient exhibits obvious nonlinearity as the roll amplitude becomes larger than 4.0°.
- For a free decay test of a vessel with half-filled spherical tanks, the liquid cargo motion is observed to increase the linear component of roll damping, but to reduce the quadratic component. In future, it is worth studying whether the same holds for other filled conditions.
- Non-linearity in roll damping should be accounted for when predicting the extreme roll response in numerical simulations.
- Flow memory effect is not important for the roll damping in a free decay test.
- Bilge keels affect the roll damping mainly through the quadratic component of the roll damping.

In this study, the nonlinear damping characteristics of a barge-like vessel with liquid cargo effects in spherical tanks were studied for the first time. The results are expected to contribute in the estimation of the operational availability for the side-by-side offloading.

Acknowledgments

This work was funded by Shell and conducted in the Deepwater Offshore Basin at Shanghai Jiao Tong University as a joint program with the University of Western Australia. The first author is supported by the Shell EMI offshore engineering initiative at the University of Western Australia. Shell would like to acknowledge the support and dedication of the staff at the Shanghai Jiao Tong University Deepwater Offshore Basin.

References

[1] S. Blagoveshchenskiĭ, Theory of Ship Motions, Dover Publications, 1962, p. 649.
[2] R. Bhattacharyya, Dynamics of Marine Vehicles, JohnWiley & Sons, Inc., 1978, p. 508.
[3] S. Chakrabarti, Offshore Structure Modeling(Advanced Series on Ocean Engineering-Volume 9), World Scientific, 1994, p. 492.
[4] S. Chakrabarti, Ocean Eng. 28 (2001) 915–932.
[5] J.P.F. Denise, Trans. R. Inst. Naval Archit. 125 (1983) 255–268.
[6] M.J. Downie, P.W. Bearman, J.M.R. Granham, J. Fluid Mech. 189 (1988) 243–264.
[7] A.C. Fernandes, A.C. Oliveira, J. Mar. Sci. Appl. 8 (2009) 144–150.
[8] Y. Ikeda, Y. Himeno, N. Tanaka, A Prediction Method for Ship Roll Damping, Department of Naval Architecture, University of Osaka Prefecture, 1978 Report No. 00405.
[9] Y. Ikeda, Mar. Technol. 41 (2) (2004) 89–93.
[10] E.B. Malta, R.T. Goncalves, F.T. Matsumoto, E.R. Pereira, A.L.C. Fujarra, K. Nishimoto, Proceedings of the 29th International Conference on Ocean, Offshore and Arctic Engineering, June 6-11, 2010, Shanghai, China, 2010.
[11] J.N. Newman, Marine Hydrodynamics, The Massachusetts Institue of Technology, 1978, p. 432.
[12] R.W. Robinson, A.W. Stoddart, The Royal Institution of Naval Architect, April Meeting, 1986, pp. 65–78.
[13] N. Salvesen, E. Tuck, O. Faltinsen, The Society of Naval Architects and Marine Engineers, Annual Meeting, No. 6, 1970.
[14] S. Surendran, S. Lee, J. Reddy, G. Lee, Ocean Eng. 32 (14) (2005) 1818–1828.
[15] N. Tanaka, J. Soc. Nav. Arch, Jpn. 1961 (109) (1961) 205–212.
[16] M. Taylan, Ocean Eng. 27 (9) (2000) 921–932.
[17] R. van Veer, F. Fathi, J.G. Kherian, Proceedings of the ASME 2011 30th International Conference on Ocean, Offshore and Arctic Engineering, June 19-24, 2011, Rotterdam, The Netherlands, 2011.
[18] X. Wu, L. Tao, Y. Li, J. Offshore Mech. Arct. Eng. 127 (2005) 205–211.
[19] E.L. Wilson, Three dimensional static and dynamic analysis of structures, Computers and Structures Inc., 1995 University Avenue, Berkeley, California USA, 2000 94704.
[20] 26th ITTC Specialist Committee, International Towing Tanks Conference, 2011 2011, No. 7.5-02-07-04.5.
[21] W. Zhao, J. Yang, Z. Hu, Y. Wei, Ocean Eng. 38 (14-15) (2011) 1555–1567.